Failure mechanisms in coupled soil-foundation systems

Emina Hadzalic, Adnan Ibrahimbegovic, Samir Dolarevic

Coupled Systems Mechanics, *Vol. 7, No. 1 (2018) 27-42*
DOI: https://doi.org/10.12989/csm.2018.7.1.027

Failure mechanisms in coupled soil-foundation systems

Emina Hadzalic[1,2a], Adnan Ibrahimbegovic[*1] and Samir Dolarevic[2b]

[1]*Université de Technologie de Compiègne/Sorbonne Universités, Laboratoire Roberval de Mecanique, Centre de Recherche Royallieu, 60200 Compiègne, France*
[2]*Faculty of Civil Engineering, University of Sarajevo, Patriotske lige 30, Sarajevo 71000, Bosnia and Herzegovina*

(Received February 25, 2017, Revised March 14, 2017, Accepted March 21, 2017)

Abstract. Behavior of soil is usually described with continuum type of failure models such as Mohr-Coulomb or Drucker-Prager model. The main advantage of these models is in a relatively simple and efficient way of predicting the main tendencies and overall behavior of soil in failure analysis of interest for engineering practice. However, the main shortcoming of these models is that they are not able to capture post-peak behavior of soil nor the corresponding failure modes under extreme loading. In this paper we will significantly improve on this state-of-the-art. In particular, we propose the use of a discrete beam lattice model to provide a sharp prediction of inelastic response and failure mechanisms in coupled soil-foundation systems. In the discrete beam lattice model used in this paper, soil is meshed with one-dimensional Timoshenko beam finite elements with embedded strong discontinuities in axial and transverse direction capable of representing crack propagation in mode I and mode II. Mode I relates to crack opening, and mode II relates to crack sliding. To take into account material heterogeneities, we determine fracture limits for each Timoshenko beam with Gaussian random distribution. We compare the results obtained using the discrete beam lattice model against those obtained using the modified three-surface elasto-plastic cap model.

Keywords: discrete beam lattice model; modified three-surface elasto-plastic cap model; Timoshenko beam; Gaussian distribution; failure mechanisms

1. Introduction

Nonlinear behavior of soil subjected to extreme loading is highly complex, with numerous factors affecting the final response. To take into account inelastic behavior and all the phenomena that can occur in different types of soils exposed to extreme loading, the phenomenological constitutive model requires a large number of parameters. For a more successful application in engineering practice, the model should be described with only few parameters that have clear physical meaning and that can be obtained from standard tests. In addition, numerical

∗Corresponding author, Chair for Computational Mechanics, Professor,
E-mail: adnan.ibrahimbegovic@utc.fr
[a]Ph.D., E-mail: emina.hadzalic@utc.fr or emina.hadzalic@gf.unsa.ba
[b]Professor, E-mail: samir.dolarevic@gf.unsa.ba

http://www.techno-press.org/?journal=csm&subpage=8 ISSN: 2234-2184 (Print), 2234-2192 (Online)

implementation of the model should give efficient performance in terms of used computational time and rates of convergence. Some of the most commonly used soil models are Mohr-Coulomb model, Drucker-Prager model, Hardening soil model, cap models etc. (DiMaggio and Sandler 1971, Hofstetter *et al*. 1993, Schanz *et al*. 1999, Doherty and Muir Wood 2013, Truty and Obrzud 2015). These models are homogenized, continuum-type models with strength and deformability defined at the macroscale. There are many problems in which these models are successfully used e.g. experimental tests simulations, deep excavations, shallow and deep foundations etc. Frequently, in the problems of soil-foundation interaction where the influence of the settlement on the response of the structure is to be analyzed, a linear elastic model of the soil is used (Chore 2014, Chore and Siddiqui 2016). The main drawback of these models is their inability to capture the post-peak behavior and failure mechanisms in soil subjected to extreme loading. This could have as a consequence of underestimating the risk of final failure.

Continuum models have been extended to take into account the softening part of the response. For modeling the failure in soils, non-local elasto-viscoplastic constitutive model has been used (Conte *et al*. 2010, 2013). In this model, a failure in soil occurs as a result of the reduction in strength parameters of the Mohr-Coulomb model with the increase in the value of plastic strain. For modeling fracturing in rocks, anisotropic viscodamage-viscoplastic consistency constitutive model with a parabolic cap has been used in which Drucker-Prager yield function and Rankine criterion have been incorporated (Saksala and Ibrahimbegovic 2014). Localized failure in saturated and partially saturated soils has been modeled by introducing a strong discontinuity in the displacement field with Drucker-Prager model governing the continuum response (Callari and Armero 2004, Callari *et al*. 2010) Embedded strong discontinuity in combination with continuum damage model has been used to model failure in rocks (Saksala *et al*. 2015, 2016).

In this paper, we propose the use of the discrete beam lattice model for predicting localized failure in soils contrary to the contiuum models. Discrete lattice models have been previously successfully used in predicting macroscale response and failure mechanisms in concrete and rocks, both in 2D and 3D setting. In discrete lattice models, a solid body is represented as an assembly of particles held together with cohesive links. Failure in a cohesive link actually means formation of a crack in the solid body. The accurate macroscale response of the solid body is obtained by proper modeling the microscale i.e. cohesive links. Truss bar elements with embedded strong discontinuity in axial direction have been used as cohesive links to model behavior and fracturing in concrete (Benkemoun *et al*. 2010, 2012). In this discrete lattice model, truss bar elements were able to fail in mode I that relates to crack opening. Beside mode I, crack can also propagate in mode II that relates to crack sliding. To be able to capture both mode I and mode II of failure, Timoshenko beam finite elements with embedded strong discontinuity in axial and transverse direction have to be used instead of truss bar elements. This type of discrete beam lattice model has been successfully used to describe behavior and fracturing in rocks (Nikolic *et al*. 2015, Nikolic and Ibrahimbegovic 2015). In the discrete beam lattice model proposed in (Nikolic *et al*. 2015), a distinction between two phases has been made. Phase I is intact rock which is not likely to fail. This phase is represented with standard linear elastic Timoshenko beam finite element. Phase II represents weak phase or initial discontinuities in rocks. Inelastic Timoshenko beam finite elements with enhanced kinematics are used to model this phase. Different types of failure mechanisms in soils are, among other, result of material heterogeneities, loading and boundary conditions.

The main novelty in this paper is to extend two-dimensional plain-strain discrete beam lattice model proposed in (Nikolic *et al*. 2015), in which all Timoshenko beams are likely to fail. Also, in

order to better take into account material heterogeneities, we determine fracture limits for each Timoshenko beam with Gaussian random distribution. We compare the results obtained with the discrete beam lattice model against those provided by a modified three-surface elasto-plastic cap model (Dolarevic and Ibrahimbegovic 2007).

The outline of the paper is as follows: In Section 2, we describe the discrete beam lattice model and give a short overview of finite element formulation for a Timoshenko beam finite element with embedded discontinuity in axial and transverse direction. In section 3, we give a short overview of modified three-surface elasto-plastic cap model. In section 4, we give a set of numerical examples where we compare the macroscale responses obtained with the discrete beam lattice model and modified three-surface elasto-plastic cap model. In section 5, we give concluding remarks.

2. Discrete beam lattice model

In the discrete beam lattice model proposed in (Nikolic *et al*. 2015) a solid body is represented as an assembly of one-dimensional Timoshenko beam finite elements with embedded strong discontinuity in axial and transverse direction capable of representing crack propagation in mode I and mode II. The meshing of the domain is done using Delaunay triangulation (Edelsbrunner 2001). Delaunay triangulation is based on the Delaunay criterion. This criterion, also called the empty circum-circle criterion, states that the cirum-circle associated with each triangle does not contain vertices of any other triangle in its interior. The end result of Delaunay triangulation is a mesh of triangles. The discrete model of a solid body is obtained by positioning Timoshenko beam finite elements along the edge of every Delaunay triangle. Cross sectional properties of the Timoshenko beams are determined from Voronoi diagram. For a given set of points, Voronoi diagram divides the region into a set of subregions or Voronoi cells. Voronoi cell is a set of all points that are the closest to the given point than to any other point. One of the most important property of the Voronoi discretization is that it can represent homogenized linear elastic responses. Here, we extend this goal further to representing the corresponding failure mechanisms. Namely, we first recall that Delaunay triangulation is dual to Voronoi cell representation. In other word, a center of every Voronoi cell is at the same time a vertex of a Delaunay triangle. For this reason, Voronoi diagram is constructed from a set of points that corresponds to the vertices of triangles obtained from the Delaunay triangulation. Each Timoshenko beam connects centers of two neighboring Voronoi cells and is perpendicular to their shared edge. The height of the cross section of any Timoshenko beam can then be determined from the length of that shared edge. This kind of cross section properties computation has been successfully used previously in (Ibrahimbegovic and Delaplace 2003). The discrete lattice model constructed in this way can successfully reproduce the linear elastic response of the equivalent standard continuum model as shown in (Nikolic *et al*. 2015). What needs to be emphasized is that the center of the Timoshenko beam is located at the edge shared between two neighboring Voronoi cells. This is a very convenient property for simulating crack propagation in materials. If we see Voronoi cells as parts of the material that are held together with cohesive links, then cracks in mode I and/or mode II can only occur at their interconnection. Next, we give governing equations for inelastic Timoshenko beam with enhanced kinematics. More details can be found in (Ibrahimbegovic 2009, Nikolic *et al*. 2015, Nikolic and Ibrahimbegovic 2015, Do *et al*. 2015, Imamovic *et al*. 2015).

2.1 Kinematics

Consider a standard, straight Timoshenko beam finite element of a length L^e and cross section A^e. The element has two nodes with three degrees of freedom at each node: axial displacement, transverse displacement and rotation of cross section. To represent crack propagation in mode I and mode II, strong discontinuities are introduced both in axial and in transverse directions. Interpolation of displacement fields in matrix notation is written

$$\mathbf{u} = \mathbf{N}\mathbf{d} + M\boldsymbol{\alpha} \tag{1}$$

$$\mathbf{N} = \begin{bmatrix} N_1 & 0 & 0 & N_2 & 0 & 0 \\ 0 & N_1 & 0 & 0 & N_2 & 0 \\ 0 & 0 & N_1 & 0 & 0 & N_2 \end{bmatrix}, \{N_1, N_2\} = \left\{1 - \frac{x}{L^e}, \frac{x}{L^e}\right\}, \mathbf{d} = \begin{Bmatrix} u_1 \\ v_1 \\ \theta_1 \\ u_2 \\ v_2 \\ \theta_2 \end{Bmatrix}, \boldsymbol{\alpha} = \begin{Bmatrix} \alpha_u \\ \alpha_v \\ 0 \end{Bmatrix} \tag{2}$$

$$M(x) = \begin{cases} -N_2(x), & x \in [0, \bar{x}] \\ H_{\bar{x}} - N_2(x), & x \in [\bar{x},\ 1] \end{cases}, \ H_{\bar{x}} = \begin{cases} 0, & x \le \bar{x} \\ 1, & x > \bar{x} \end{cases} \tag{3}$$

Interpolation of deformation fields in matrix notation is written

$$\boldsymbol{\varepsilon} = \mathbf{B}\mathbf{d} + G\boldsymbol{\alpha} \tag{4}$$

$$\mathbf{B} = \begin{bmatrix} B_1 & 0 & 0 & B_2 & 0 & 0 \\ 0 & B_1 & -N_1 & 0 & B_2 & -N_2 \\ 0 & 0 & B_1 & 0 & 0 & B_2 \end{bmatrix}, \ \{B_1, B_2\} = \left\{-\frac{1}{L^e}, \frac{1}{L^e}\right\} \tag{5}$$

$$G(x) = \frac{dM(x)}{dx} = \begin{cases} -\dfrac{1}{L^e}, & x \in [0, \bar{x}) \cup (\bar{x}, L^e] \\ -\dfrac{1}{L^e} + \delta_{\bar{x}}, & x = \bar{x} \end{cases} \tag{6}$$

where $\delta_{\bar{x}}$ is the Dirac function

$$\delta_{\bar{x}} = \begin{cases} 0, & x \in [0, \bar{x}) \cup (\bar{x}, L^e] \\ \infty, & x = \bar{x} \end{cases} \tag{7}$$

2.2 Equilibrium

The equilibrium equations are derived from the principle of virtual work, which states that the body is in equilibrium if virtual works of internal and external forces are equal. Taking into account the contribution of each element to the global equilibrium, we get two sets of equations. The first represents the equilibrium in the bulk, and the second represents the equilibrium at the discontinuity.

$$\mathop{\mathrm{A}}_{e=1}^{n} \left[\mathbf{f}^{int,e} - \mathbf{f}^{ext,e} \right] = \mathbf{0} \tag{8}$$

$$\forall e : \mathbf{h}^e = \mathbf{0} \tag{9}$$

2.3 Constitutive equations

The constitutive law for a Timoshenko beam finite element in axial and transverse direction consists of three parts (Fig. 1). The first part is the linear elastic part described with Hooke's linear elastic law. After reaching the yield limit, the behavior of the element is governed by plasticity with linear isotropic hardening. Post-peak behavior of an element is described with exponential softening. Behavior of the element in bending in all three parts is linear elastic.

Governing equations for plasticity with linear isotropic hardening:

-Additive decomposition of total deformation in elastic ε^e and plastic part ε^p:

$$\varepsilon = \varepsilon^e + \varepsilon^p$$

-Strain energy function in terms of strains ε and internal variables, plastic deformation ε^p and strain-like hardening variable ξ:

$$\psi\left(\varepsilon, \varepsilon^p, \xi\right) = \frac{1}{2}\left(\varepsilon - \varepsilon^p\right) C \left(\varepsilon - \varepsilon^p\right) + \frac{1}{2} \xi K \xi$$

where C is the elastic constant (E or G), and K the hardening modulus.

-Yield function in terms of stress σ and dual variable q:

$$\phi(\sigma, q) = |\sigma| - \left(\sigma_y - q\right) \leq 0$$

where σ_y is the yield limit, and $q = -K\xi$ is a stress-like variable.

-Evolution equations for internal variables ε^p and ξ:

$$\frac{\partial \varepsilon^p}{\partial t} = \frac{\partial \overline{\gamma}}{\partial t} sign(\sigma), \ \frac{\partial \xi}{\partial t} = \frac{\partial \overline{\gamma}}{\partial t}$$

where $\overline{\gamma}$ is the plastic multiplier.

-Loading/unloading conditions:

$$\frac{\partial \overline{\gamma}}{\partial t} \geq 0, \ \phi \leq 0, \ \frac{\partial \overline{\gamma}}{\partial t} \phi = 0$$

-Consistency condition:

$$\frac{\partial \overline{\gamma}}{\partial t} \frac{\partial \phi}{\partial t} = 0$$

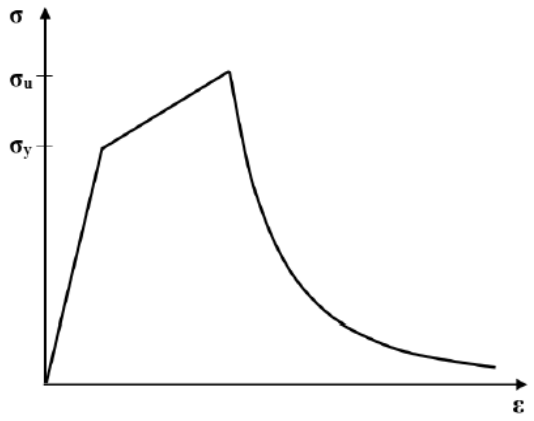

Fig. 1 Constitutive model for Timoshenko beam finite element for axial and transverse direction

Governing equations for exponential softening:

-Yield function in terms of stress σ and dual variable $\bar{\bar{q}}$:

$$\bar{\bar{\phi}}\left(\mathrm{t},\bar{\bar{q}}\right)=|\sigma|-\left(\sigma_u-\bar{\bar{q}}\right)\le 0$$

where t is the internal force acting at the discontinuity.

-Stress-like softening variable $\bar{\bar{q}}$ for exponential softening:

$$\bar{\bar{q}}=\sigma_u\left(1-exp\left(-\bar{\bar{\xi}}\frac{\sigma_u}{G_f}\right)\right)$$

where σ_u is the ultimate stress, and G_f is the fracture energy.

-Evolution equations for internal variables, displacement jump α and strain-like softening variable $\bar{\bar{\xi}}$:

$$\frac{\partial\alpha}{\partial t}=\frac{\partial\bar{\bar{\gamma}}}{\partial t}sign\left(\mathrm{t}\right),\ \frac{\partial\bar{\bar{\xi}}}{\partial t}=\frac{\partial\bar{\bar{\gamma}}}{\partial t}$$

where $\bar{\bar{\gamma}}$ is the plastic multiplier.

-Loading/unloading conditions:

$$\frac{\partial\bar{\bar{\gamma}}}{\partial t}\ge 0,\ \bar{\bar{\phi}}\le 0,\ \frac{\partial\bar{\bar{\gamma}}}{\partial t}\bar{\bar{\phi}}=0$$

-Consistency condition:

$$\frac{\partial\bar{\bar{\gamma}}}{\partial t}\frac{\partial\bar{\bar{\phi}}}{\partial t}=0$$

3. Modified three-surface elasto-plastic cap model

The yield function of a cap model consists of three surfaces. The first surface is Drucker-Prager frictional failure envelope, which defines the shear strength of the material. The position of the Drucker-Prager failure envelope is fixed in stress space. The second surface of the cap model is a strain-hardening cap in compression. The position of the cap in stress space is defined with the current value of plastic volumetric strain. The cap can be of a circular or elliptical shape. Also, the cap in a form of vertical line with behavior governed by damage model instead of plasticity has also been used (Ibrahimbegovic *et al*. 2003). In order to limit tensile stresses to the value of the tensile strength of the soil, a cut-off plane is introduced as a third surface of the cap model. The yield function of a cap model at the intersection of these surfaces is not smooth, which causes difficulties in numerical computation due to singularity of the tangent operator in the corner regions (Fig. 2(a)). For this reason in (Dolarevic and Ibrahimbegovic 2007), a modified version of the cap model is proposed in which the intersection point of the elliptic cap and failure cone is moved to the point where the tangent line of the ellipse coincides with the meridian of the cone. In order to eliminate the second corner region, the cut-off plane is replaced by a circle (Fig. 2(b)). These modifications result in a smooth yield function, which ensures efficient numerical performance of the model without big changes in the behavior compared to the non-smooth cap models. Formulation of the cap models is usually given in I_1 - $\sqrt{J_2}$ diagram, where I_1 is the first invariant of the stress tensor and J_2 is the second invariant of the deviatoric part of the stress tensor. The first invariant of the stress tensor I_1 controls the volumetric deformations of the

specimen, while the second invariant of the deviatoric part J_2 controls the change in the shape of the specimen.

$$I_1 = tr[\boldsymbol{\sigma}] \tag{10}$$

$$\sqrt{J_2} = \|\mathrm{dev}[\boldsymbol{\sigma}]\| \tag{11}$$

The Drucker-Prager loading function for the modified cap model is written as

$$f_1(I_1, J_2) = \alpha I_1 + \sqrt{J_2} - k = 0,\ I_1^T \le I_1 \le I_1^c \tag{12}$$

where α and k are strength parameters specifying soil cohesion and angle of internal friction.

The strain-hardening elliptic cap function is written as

$$f_2\left(I_1, J_2, \xi\left(\varepsilon_v^p\right)\right) = \frac{(I_1 - a)^2}{R^2 f_{dp}(a)} + J_2 - \mathrm{b}^2 = 0,\ I_1 \ge I_1^c \tag{13}$$

where $\xi\left(\varepsilon_v^p\right)$ is the hardening law defined with

$$\xi\left(\varepsilon_v^p\right) = \frac{1}{D} ln\left(1 + \frac{\varepsilon_v^p}{W}\right) \tag{14}$$

In previous equations, R, W and D are hardening material parameters, $a(\xi)$ is an ordinate of the ellipse center, $b(\xi)$ is the main radius of the ellipse.

The function for the third surface i.e., the cut-off plane is written as

$$f_3(I_1, J_2) = (I_1 - T + R_T)^2 = R_T^2,\ I_1 \le I_1^T \tag{15}$$

where T is the tension cut-off limit, and R_T is the radius center.

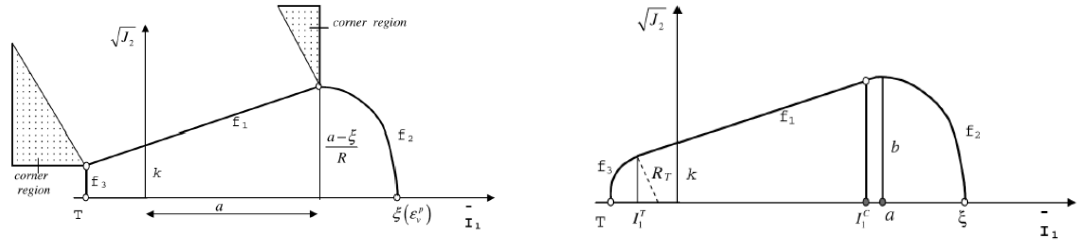

(a) (b)

Fig. 2 Cap model (a) non-smooth cap model (b) modified cap model (Dolarevic and Ibrahimbegovic 2007)

4. Numerical simulations

In this section we give the results obtained for a set of numerical examples. First, we simulate the direct shear test commonly used in geotechnical engineering to determine strength parameters of soil and weak rocks. Second, we simulate the response of the soil under both rigid and flexible footing. The mesh in all examples is generated in GMSH using Delaunay triangulation (Geuzine

and Remacle 2009). The corresponding Voronoi diagram is derived from Delaunay vertices. The area of Timoshenko beam finite element is calculated from the length of the edge shared between two neighbouring Voronoi cells. All numerical computations are preformed with the research version of the computer code FEAP, developed by R.L.Taylor (Zienkiewicz and Taylor 2005).

4.1 Direct shear test

Direct shear test is a commonly used test for determining Mohr-Coulomb strength parameters of soils and weak rocks, cohesion and angle of internal friction. We preform the direct shear test on the specimen of very stiff clay. The dimensions of the specimen are 60×25 mm with unit thickness (Fig. 3(a) and 3(b)). The mechanical properties used in numerical simulations are given in Table 1. The ultimate values of stresses are randomly assigned to every element using Gaussian random distribution with parameters: mean μ and standard deviation σ. The test is conducted in two phases (Fig. 4(a)). In the first phase, we apply normal pressure. In the second phase, we impose horizontal displacements on the upper part of the specimen while keeping the normal pressure constant.

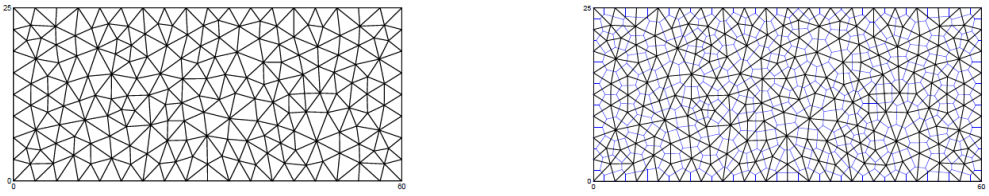

(a) (b)

Fig. 3 Discretization of the specimen (a) mesh (b) Voronoi diagram

Table 1 Mechanical properties of the Timoshenko beam finite element

Young's modulus (MPa)	Poisson's ratio	Yield limit (MPa)	Hardening modulus (MPa)	Fracture limit (MPa)	Fracture energy (N/mm)
$E=100$	$\nu=0.2$	$\sigma_{y,t}=0.18$	$K_t=5.0$	$\mu_t=0.22$ $\sigma_t=0.01$	$G_{f,t}=0.1$
		$\sigma_{y,c}=1.80$	$K_c=5.0$	$\mu_c=2.20$ $\sigma_c=0.10$	$G_{f,c}=2.0$
		$\sigma_{y,s}=0.22$	$K_s=5.0$	$\mu_s=0.26$ $\sigma_s=0.01$	$G_{f,s}=5.0$

To investigate the influence of applied normal pressure on the shear strength we repeat computation for three different values of normal pressure: 50 kPa, 100 kPa and 200 kPa. We can conclude that the increase in normal pressure results in the increase of the shear strength, as stated in Mohr-Coulomb law (Fig. 4(b)). From the obtained results, we then form a Mohr-Coulomb envelope to determine the values of cohesion and angle of internal friction of the specimen. The cohesion represents the value of the shear stress at zero normal pressure, whereas the angle of internal friction represents the slope of the Mohr-Coulombs envelope. The computed values of cohesion and angle of internal friction are 360 kPa and 23° which fall in the range of the values for very stiff clays (Fig. 4(c)). In experimental direct shear tests, the horizontal failure surface at the

mid-height of the specimen is pre-imposed with the test set-up. The formed macrocrack in numerical simulation, shown in Fig. 5, splits the specimen in two parts as in experimental direct shear tests.

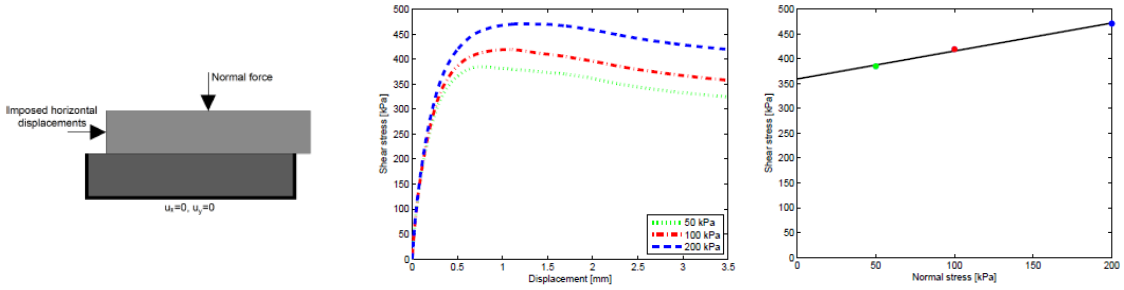

(a) (b) (c)

Fig. 4 Direct shear test: (a) loading and boundary conditions (b) computed stress - displacement curves (c) computed Mohr-Coulomb envelope

(a) (b)

Fig. 5 Elements with increasing damage (a) mode I (b) mode II (note that we mark the cohesive links that are activated by cracks)

We also preform a numerical simulation of a direct shear test on a specimen with dimensions 100×25 mm. The value of normal pressure for which we do the computation is 100 kPa. The mesh density is similar to the one used in previous computations with a total of 611 elements compared to 572 elements in the mesh shown in Fig. 3(a). In Fig. 6(a), the computed stress-displacement curves for specimens sizes 100×25 mm and 60×25 mm are shown. The specimen with dimensions 100×25 mm is slightly more resistant in the post-peak part of the response. This finding is in agreement with the probability-based explanation of the size effect (Ibrahimbegovic *et al*. 2010).

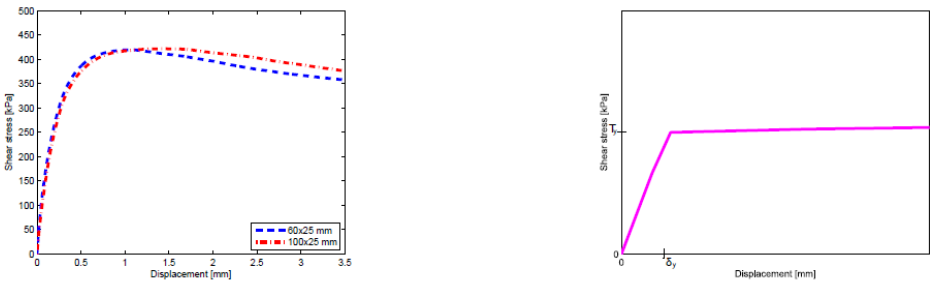

(a) (b)

Fig. 6(a) Comparison of stress-displacement curves in direct shear tests for two types of specimens (b) Typical stress-displacement curve obtained with cap model

A simulation of the shear test is also done in (Dolarevic and Ibrahimbegovic 2007) using the proposed modified cap model. In Fig. 6b, a typical stress-displacement curve is shown. After the specimen reaches shear strength, further response is governed by perfect plasticity. The cap model cannot describe the softening part of the response of the specimen i.e. the decrease in the values of stresses with the increase of the displacements after the strength of the material has been reached.

4.2 Coupled soil-foundation system

In this section, we give a numerical simulation of a rigid and flexible footing on a soil stratum. We preform the computation for a coarse mesh with 418 finite elements and a fine mesh with 1547 finite elements. The geometry, mesh and boundary conditions are shown in Figs. 7 and 8. We choose mechanical properties of the Timoshenko beam finite element in both cases by matching the computed force-displacement curve with the one obtained in (Dolarevic and Ibrahimbegovic 2007) using the modified three-surface elasto-plastic cap model. In (Dolarevic and Ibrahimbegovic 2007), the force-displacement curve is obtained for the case of the flexible footing. This has its effect on the choice of the linear elastic parameters for the Timoshenko beam finite element, which is addressed in the next subsection.

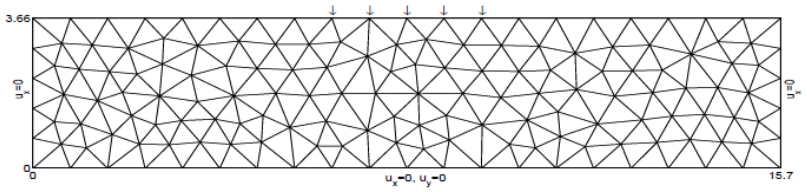

Fig. 7 Coarse mesh

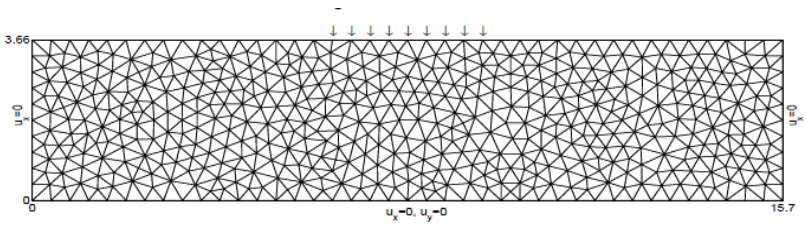

Fig. 8 Fine mesh

4.2.1 Rigid footing

Vertical displacements of a rigid footing are uniform. To simulate the response of a rigid footing, we impose uniform vertical displacement along the length of the footing. For solving the global phase of the computation, we use the Newton-Raphson method in combination with the line search alogrithm. The values of mechanical properties of the Timoshenko beam finite element obtained by matching the curve given in (Dolarevic and Ibrahimbegovic 2007) are shown in Table 2. Young's modulus for the Timoshenko beam finite element does not match the one used in (Dolarevic and Ibrahimbegovic 2007) and is somewhat smaller. This is due to different loading conditions because the computation in (Dolarevic and Ibrahimbegovic 2007) is carried out for the case of flexible footing.

Table 2 Mechanical properties of the Timoshenko beam finite element

Young's modulus (MPa)	Poisson's ratio	Yield limit (MPa)	Hardening modulus (MPa)	Fracture limit (MPa)	Fracture energy (MN/m)
$E=160$	$v=0.3$	$\sigma_{y,t}=0.03$	$K_t=60$	$\sigma_{u,t}=0.09$	$G_{f,t}=0.0006$
		$\sigma_{y,c}=0.30$	$K_c=60$	$\sigma_{u,c}=0.90$	$G_{f,c}=0.06$
		$\sigma_{y,s}=0.07$	$K_s=60$	$\sigma_{u,s}=0.13$	$G_{f,s}=0.02$

Computed reaction-displacement curves are shown in Fig. 9. Linear elastic parts of the responses for the coarse and the fine mesh do not differ significantly. After first cracks start to form, responses for two different types of the mesh start to differ in the end resulting with the different ultimate load values. In the post-peak behavior, a macrocrack of a similar pattern is formed in both cases, leading to the failure of soil under the footing. The macrocrack propagation occurs dominantly in mode II in the case of the coarse mesh, whereas in the case of the fine mesh macrocrack propagation occurs in both modes I and II. The shape of the formed macrocrack under the footing corresponds to the commonly observed shape of the failure wedge (Figs. 10, 11).

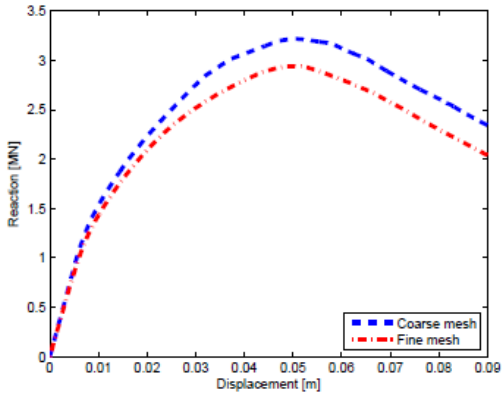

Fig. 9 Comparison of computed force-displacement curves for rigid footing

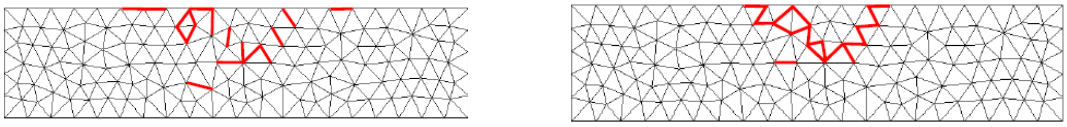

(a) (b)

Fig. 10 Coarse mesh: Elements with increasing damage (a) mode I (b) mode II

(a) (b)

Fig. 11 Fine mesh: Elements with increasing damage (a) mode I (b) mode II

Computed reaction-displacement curves are shown in Fig. 9. Linear elastic parts of the responses for the coarse and the fine mesh do not differ significantly. After first cracks start to form, responses for two different types of the mesh start to differ in the end resulting with the different ultimate load values. In the post-peak behavior, a macrocrack of a similar pattern is formed in both cases, leading to the failure of soil under the footing. The macrocrack propagation occurs dominantly in mode II in the case of the coarse mesh, whereas in the case of the fine mesh macrocrack propagation occurs in both modes I and II. The shape of the formed macrocrack under the footing corresponds to the commonly observed shape of the failure wedge (Figs. 10, 11).

4.2.2 Flexible footing

Contact pressure distribution under flexible footing is uniform. To simulate the response of a flexible footing, we apply forces at the nodes along the length of the footing. For solving the global phase of the computation, we use the arclength method. The values of mechanical properties of the Timoshenko beam finite element obtained by matching the curve given in (Dolarevic and Ibrahimbegovic 2007) are shown in Table 3. Computed reaction-displacement curves are shown in Fig. 12. Linear elastic parameters of the Timoshenko beam finite element, Young's modulus and Poisson's coefficient, match the linear elastic parameters used for the computation of the response under the flexible footing in (Dolarevic and Ibrahimbegovic 2007). This confirms that the discrete beam lattice model can successfully reproduce the linear elastic part of the reponse of an equvivalent continuum model. With the appropriate selection of mechanical properties of the Timoshenko beam finite elements, the discrete beam lattice model can also closely match the plastic part of the response and predict the value of ultimate load. Contrary to the continuum model, with the discrete beam lattice model we are able to capture the post-peak behavior and failure mechanisms.

Table 3 Mechanical properties of the Timoshenko beam finite element

Young's modulus (MPa)	Poisson's ratio	Yield limit (MPa)	Hardening modulus (MPa)	Fracture limit (MPa)	Fracture energy (MN/m)
$E=205$	$\nu=0.3$	$\sigma_{y,t}=0.04$	$K_t=60$	$\mu_t=0.113$ $\sigma_t=0.005$	$G_{f,t}=0.0006$
		$\sigma_{y,c}=0.40$	$K_c=60$	$\mu_c=1.130$ $\sigma_c=0.05$	$G_{f,c}=0.05$
		$\sigma_{y,s}=0.07$	$K_s=60$	$\mu_s=0.133$ $\sigma_s=0.005$	$G_{f,s}=0.02$

Computed responses obtained with the discrete beam lattice model prior to reaching the ultimate load level are practically mesh-independent. In the post-peak part of the response, in the case of a coarse mesh, a macrocrack has formed resulting in the decrease of the load carrying capacity of the soil under the footing (Fig. 13). In the case of fine mesh, a macrocrack was not formed due to localized failure in elements, thus the softening part of the response could not be captured (Fig. 14).

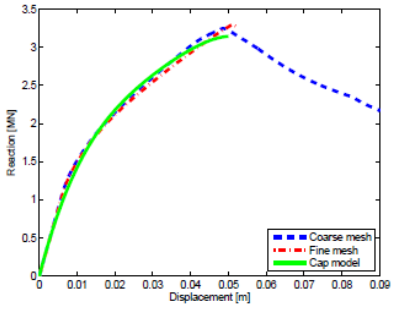

Fig. 12 Comparisson of the computed force-displacement curve with the curve provided by the modified cap model for flexible footing

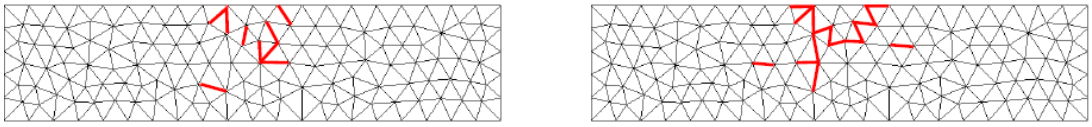

(a) (b)

Fig. 13 Coarse mesh: Elements with increasing damage (a) mode I (b) mode II

(a) (b)

Fig. 14 Fine mesh: Elements with increasing damage (a) mode I (b) mode II

In the Fig. 15, stress states under footing obtained with the modified cap model in (Dolarevic and Ibrahimbegovic 2008) are shown. We can conclude that a failure wedge of similar shape as in the case of the discrete model is also noticed. However, the plastic zone in the cap model is smeared across a large area of the domain.

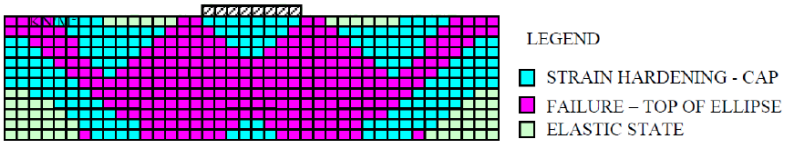

Fig. 15 Stress state under footing for modified cap model (Dolarevic and Ibrahimbegovic 2008)

To compare the results for rigid and flexible footing, we repeat computation for flexible footing with the values of mechanical properties of the Timoshenko beam finite element given in table 2. From computed curves, shown in figure 16, we can state that the value of ultimate load is higher in the case of a rigid footing. We can also conclude that the response of the discrete beam lattice model exibits some mesh dependency. A certain level of mesh-dependency is also observed in the continuum model in (Dolarevic and Ibrahimbegovic 2007).

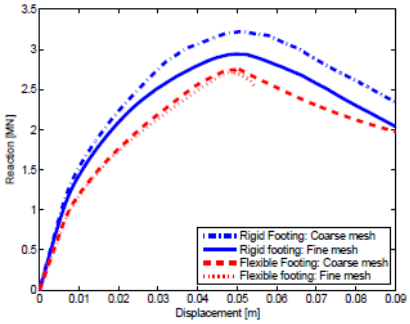

Fig. 16 Comparison of computed force-displacement curves for rigid and flexible footing

5. Conclusions

In this paper we used a discrete beam lattice model based on inelastic Timoshenko beam finite elements with enhanced kinematics to describe the response and failure mechanisms in coupled soil-foundation system. The soil model is constructed with Voronoi cells, with cohesive links represented by Timoshenko beams. We have shown that with the appropriate selection of parameters of Timoshenko beam finite elements, the discrete beam lattice model is able to reproduce the reponse of an equivalent continuum model and predict the corresponding ultimate load value. However, the proposed discrete model can also describe post-peak behavior and capture failure mechanisms in soil subjected to footing load. Thus, we can obtain the ultimate load in (much) more solvable manner, without any ambiguity between the (potential) lack of convergence and real peak resistance.

The advantage of this discrete beam lattice model is that the true failure modes are captured with one-dimensional elements. This ensures relativly simple and efficient numerical implementation of the model. One of the drawbacks of these models is that some of the parameters for Timoshenko beam finite elements can not be obtained directly as a result of experimental tests, but rather more elaborate parameter identification methods should be used where material heterogenities can also play a role. The discrete beam lattice models also represent a good basis for the application of probability methods from which probability density function of soil collapse can be predicted. The models of this kind can provide the sound, probability-based explanation of size effect, where the ultimate load and failure mechanisms are affected by the size of the structure.
Because the response of the soil is highly influenced by the presence of water, in future works we plan to study the influence of coupling between soil and fluid on the behavior and failure mechanisms in coupled soil-foundation systems.

Acknowledgments

This work was supported by the French Ministry of Foreign Affairs and French Embassy in Bosnia and Herzegovina. Professor Adnan Ibrahimbegovic was supported by funding for Chaire de Mécanique Picardie (120-2015 RDISTRUCT-000010 and RDISTRUCT-000010) and EU funding (FEDER). This support is gratefully acknowledged. We also acknowledge many helpful discussions with Dr. M. Nikolic.

References

Benkemoun, N., Hautefeuille, M., Colliat J.B. and Ibrahimbegovic, A. (2010), "Failure of heterogeneous materials: 3D meso-scale FE models with embedded discontinuities", *J. Numer. Meth. Eng.*, **2010**(82), 1671-1688.

Benkemoun, N., Ibrahimbegovic, A. and Colliat, J.B. (2010), "Anisotropic constitutive model of plasticity capable of accounting for details of meso-structure of two-phase composite material", *Comput. Struct.*, **2012**(90), 153-162.

Callari, C. and Armero, F. (2004), "Analysis and numerical simulation of strong discontinuities in finite strain poroplasticity", *Comput. Meth. Appl. Mech. Eng.*, **2004**(193), 2941-2986.

Callari, C., Armero, F. and Abati, A. (2010), "Strong discontinuities in partially saturated poroplastic solids", *Comput. Meth. Appl. Mech. Eng.*, **2010**(199), 1513-1535.

Chore, H.S. (2014), "Interactive analysis of a building fame resting on pile foundation", *Coupled Syst. Mech.*, **2014**(3), 367-384.

Chore, H.S. and Siddiqui, M.J. (2016), "Soil-structure interaction analysis of a building frame supported on piled raft", *Coupled Syst. Mech.*, **2016**(5), 41-58.

Conte, E., Donato, A. and Torncone, A. (2013), "Progressive failure analysis of shallow foundations on soils with strain-softening behaviour", *Comput. Geotech.*, **2013**(54), 117-124.

Conte, E., Silvestri F. and Torncone A. (2010), "Stability analysis of slopes in soils with strain-softening behaviour", *Comput. Geotech.*, **2010**(37), 710-722.

DiMaggio, F.L. and Sandler, I.S. (1971), "Material models for granular soils", *J. Eng. Mech. Div.*, **1971**(97), 935-950.

Do, X.N., Ibrahimbegovic, A. and Brancherie, D. (2015), "Combined hardening and localized failure with softening plasticity in dynamics", *Coupled Syst. Mech.*, **2015**(4), 115-136.

Doherty, J.P. and Muir Wood, D. (2015), "An extended Mohr-Coulomb (EMC) model for predicting the settlement of shallow foundations on sand, *Géotech.*, **2013**(63), 661-673.

Dolarevic, S. and Ibrahimbegovic, A. (2008), "Nonlinear behavior of soil as the source of structure damages", *Proceedings of the NATO-ARW Damage Assessment and Reconstruction after Natural Disasters and Previous Military Activities*, Sarajevo, October.

Dolarevic, S. and Ibrahimbegovic, A. (2007), "A modified three-sruface elasto-plastic cap model and its numerical implementation", *Comput. Struct.*, **2007**(85), 419-430.

Edelsbrunner, H. (2001), *Geometry and Topology for Mesh Generation*, Cambridge University Press.

Geuzaine, C. and Remache, J.F. (2009), "Gmsh: A 3-D finite element mesh generator with built-in pre- and post-processing facilities", *J. Numer. Meth. Eng.*, **2009**(79), 1309-1331.

Hofstetter, G., Simo, J.C. and Taylor, R.L. (1993), "A modified cap model: Closest point solution alghoritms", *Comput. Struct.*, **1993**(48), 203-214.

Ibrahimbegovic, A. (2009), *Nonlinear Solid Mechanics: Theoretical Formulations and Finite Element Solution Methods*, Springer.

Ibrahimbegovic, A., Colliat, J.B., Hautefeuille, M., Brancherie, D. and Melnyk S. (2010), "Probability based size effect representation for failure in civil engineering structures built of heterogeneous materials", *Comput. Meth. Stochast. Dyn.*, **2010**(22), 291-313.

Ibrahimbegovic, A. and Delaplace, A. (2003), "Microscale and mesocale discrete models for dynamic fracture of structures built of brittle material", *Comput. Struct.*, **2003**(81), 1255-1265.

Ibrahimbegovic, A., Markovic, D. and Gatuingt, F. (2003), "Constitutive model of coupled damage-plasticity and its finite element implementation", *Revue Eurpéenne des Eléments Finis*, **2003**(12), 381-405.

Imamovic, I., Ibrahimbegovic, A., Knopf-Lenoir, C. and Mesic, E. (2015), "Plasticity-damage model parameters identification for structural connections", *Coupled Syst. Mech.*, **2015**(4), 337-364.

Nikolic, M. and Ibrahimbegovic, A. (2015), "Rock mechanics model capable of representing initial heterogeneities and full set of 3D failure mechanisms", *Comput. Meth. Appl. Mech. Eng.*, **2015**(290), 209-227.

Nikolic, M., Ibrahimbegovic, A. and Miscevic, P. (2015), "Brittle and ductile failure of rocks: Embedded discontinuity approach for representing mode I and mode II failure mechanisms", *J. Numer. Meth. Eng.*, **2015**(102), 1507-1526.

Saksala, T., Brancherie, D., Harari, I. and Ibrahimbegovic, A. (2015), "Combined continuum damage-embedded discontinuity model for explicit dynamic fracture analyses of quasi-brittle materials", *J. Numer. Meth. Eng.*, **2015**(101), 230-250.

Saksala, T., Brancherie, D. and Ibrahimbegovic, A. (2016), "Numerical modeling of dynamic rock fracture with a combined 3D continuum viscodamage-embedded discontinuity model", *J. Numer. Anal. Meth. Geomech.*, **2016**(40), 1339-1357.

Saksala, T. and Ibrahimbegovic, A. (2014), "Anisotropic viscodamage-viscoplastic consistency constitutive model with a parabolic cap for rocks with brittle and ductile behavior", *J. Rock Mech. Min. Sci.*, **2014**(70), 460-473.

Schanz, T., Vermeer, P.A. and Bonnier, P.G. (1999), "The Hardening soil model: Formulation and verification", *Proceedings of the Plaxis-Symposium: Beyond 2000 in Computational Geotechnics*, Amsterdam, **1999**, 281-296.

Truty, A. and Obrzud, R. (2015), "Improved formulation of the hardening soil model in the context of modeling the undrained behavior of cohesive soils", *Stud. Geotech. Mech.*, 2**015**(37), 61-68.

Zienkiewicz, O.C. and Taylor, R.L. (2005), *The Finite Element Method, Vols. I, II, III*, Elsevier.

AI